THE ASTROPHYSICAL JOURNAL, 462:L53–L57, 1996 May 10

HUBBLE SPACE TELESCOPE OBSERVATIONS OF THE GRAVITATIONAL LENS SYSTEM B1422+231

C. D. IMPEY
Steward Observatory, University of Arizona, Tucson, AZ 85721; cimpey@as.arizona.edu
C. B. FOLTZ
Multiple Mirror Telescope Observatory, University of Arizona, Tucson, AZ 85719; cfoltz@as.arizona.edu
C. E. PETRY
Steward Observatory, University of Arizona, Tucson, AZ 85721; cpetry@as.arizona.edu
I. W. A. BROWNE
Nuffield Radio Astronomy Laboratories, Jodrell Bank, Cheshire SK11 9DL, England, UK; iwb@jb.man.ac.uk
AND
A. R. PATNAIK
Max-Planck-Institut für Radioastronomie, Auf dem Hügel 69, D-53121 Bonn, Germany; apatnaik@mpifr-bonn.mpg.de
Received 1995 December 6; accepted 1996 February 20

ABSTRACT

Hubble Space Telescope observations of the gravitational lens system B1422+231 are presented. The spectra of the four components are virtually identical, although there are differences among the Lyα emission-line equivalent widths that might be due to microlensing. There are also significant differences between the component flux density ratios measured at radio and optical wavelengths. High-resolution imaging reveals the lens close to the faintest quasar image. The lens has photometric properties consistent with an elliptical galaxy at $z \sim 0.4$. The addition of new constraints to simple lensing models affirms the B1422+231 system as a suitable tool for an eventual direct measure of the Hubble constant.

Subject heading: gravitational lensing

1. INTRODUCTION

On rare occasions, inhomogeneities in the universe produce multiple images of a background quasar. Such systems are extremely useful cosmological tools. In a well-modeled system where the source is variable and a time delay can be measured, a direct determination of the distance scale is possible (Refsdal 1964). Radio surveys have a yield of roughly one lens per 500 sources (Patnaik et al. 1992b), and surveys currently underway will generate about two dozen new lens systems. Such a sample can potentially be used for the determination of both the Hubble constant and the other parameters of the standard cosmological model.

The radio source B1422+231 was found to have four unresolved components within a region of diameter 1.″3 by Patnaik et al. (1992a). A similar configuration of four images has been observed at optical (Remy et al. 1993; Yee & Ellingson 1994) and infrared wavelengths (Lawrence et al. 1992). The source is a luminous quasar at $z = 3.62$. The lens has been imaged with difficulty from the ground (Yee & Ellingson 1994) and has a tentative redshift of $z = 0.65$ (Hammer et al. 1995). Global VLBI observations at 5 GHz reveal extended structures for the three brightest components (Patnaik & Porcas 1995). The attraction of B1422+231 lies in the fact that a simple model with an elliptical potential (and some shear from two other galaxies in the field) can reproduce the image configuration and the component flux ratios reasonably well (Hogg & Blandford 1994; Korman, Schneider, & Bartelmann 1994). The VLBI structures and potential proper motions of the VLBI components offer additional constraints. The source is intrinsically variable at radio wavelengths (Patnaik & Porcas 1995), with anticipated time delays of order hours to days between the three brightest components (Hogg & Blandford 1994). If one or more time delays are measured, and the mass distribution of the lens is understood, the B1422+231 system will be useful for cosmological tests.

We present observations that conclusively demonstrate that B1422+231 is a four-component gravitational lens. Spectra of the four optical components are virtually identical. High-resolution optical imaging clearly reveals the lens at the anticipated position, close to the faintest quasar component. New constraints on the lensing geometry are provided by the position, color, and ellipticity of the lensing galaxy (we assume $H_0 = 100$ kms^{-1} Mpc^{-1}, $q_0 = 0.5$).

2. OBSERVATIONS

2.1. *Images*

Two-color imaging of B1422+231 was obtained with the Faint Object Camera (FOC) on the *Hubble Space Telescope* (*HST*) (post-COSTAR) using the F/96 aperture and 256 × 256 pixel format, which results in a plate scale of 0.″01435 pixel^{-1}. One exposure was made on 1995 April 20 at 20:58:54 (UT) for 496.^{s}5 using the long-pass "*V*" filter F480LP, which has a peak wavelength of 5100 Å and a bandwidth of 744 Å; the other image was exposed for 1641.^{s}5 on 1995 April 21 at 21:31:01 (UT), using wide band "*U*" filter F342W, which has a peak wavelength of 3410 Å and a bandwidth of 702 Å. The images were processed and calibrated using STScI's Routine Science Data Processing, or "pipeline." Figure 1 (Plate L5) presents two versions of the

[1] Based on observations made with the NASA/ESA *Hubble Space Telescope*, obtained at the Space Telescope Science Institute, which is operated by AURA, Inc., under NASA Contract NAS 5-26555.

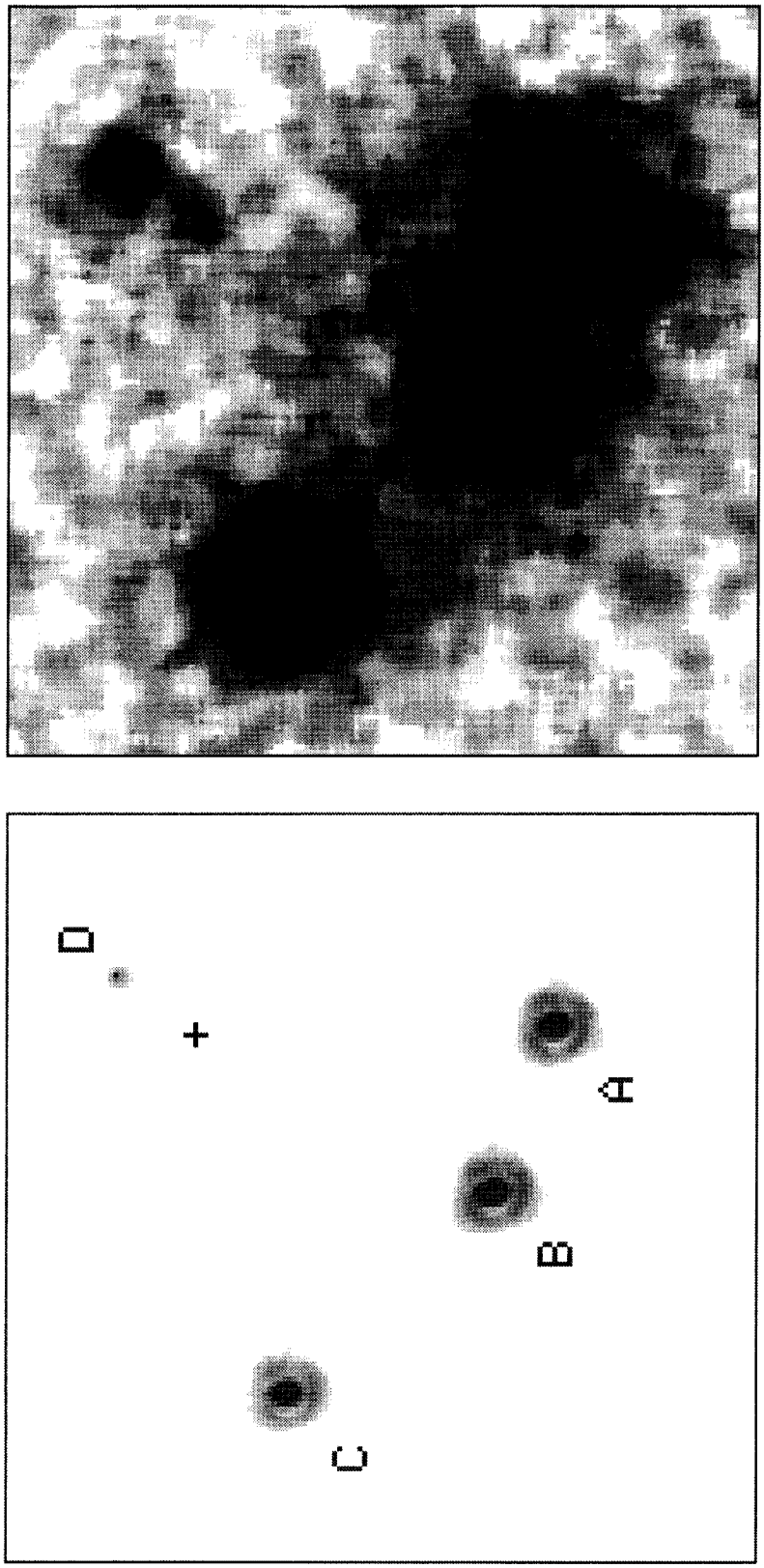

FIG. 1.—The left-hand panel shows the F480LP FOC image of the B1422+231 system, with the gray scale set to show the image cores. The image is rotated at position angle 160° from north. The cross marks the expected position of the lens according to the model of Korman et al. (1994). The right-hand panel is scaled to show the lensing galaxy.

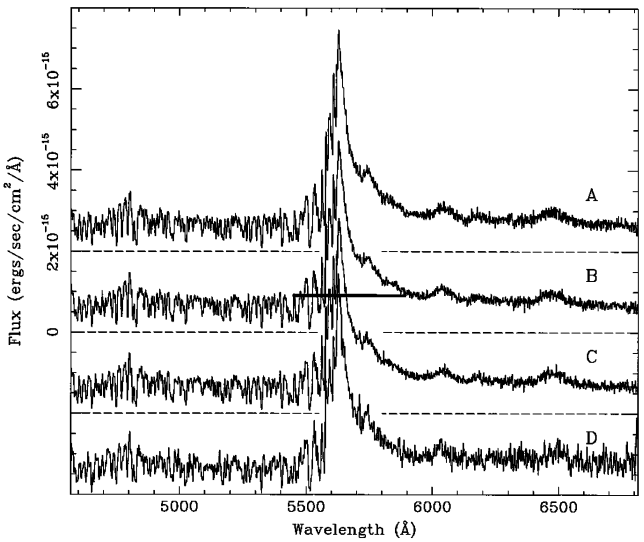

FIG. 2.—Flux-calibrated FOS spectra of B1422+231 components A–D taken through a 0.″26 diameter circular aperture. The flux scale is appropriate for image B and the other spectra are scaled using the continuum flux ratios given in Table 3. The spectrum of image D has been smoothed with a 3 pixel wide median filter. The solid line under the Lyα + N v emission in the spectrum of B shows the adopted continuum level; the endpoints of the line give the limits of integration for the equivalent width measurements.

F480LP image, one showing the cores of the bright quasar components, the other revealing the lensing galaxy.

2.2. *Spectra*

Spectra of each of the components of the lensed image of the quasar were obtained on 1995 March 27, at 15:08:46, 14:42:27, 16:30:49, and 18:14:54 (UT) for components A–D respectively, with *HST*'s Faint Object Spectrograph (FOS) using the red Digicon detector and the 0.″26 (diameter) circular aperture. Grating G570H gives a dispersion of 1.09 Å pixel^{-1}, spectral resolution of 4.15 Å (FWHM), and spectral coverage from 4569 to 6818 Å, which at the redshift of the quasar includes Lyα emission and a portion of the Lyα "forest." Total exposure time on images A–D was, respectively, 1200, 1200, 2400, and 4800 s. The data reduction was performed by STScI's "pipeline," and the individual spectra are displayed in Figure 2.

3. RESULTS

3.1. *Astrometry*

The Faint Object Camera (FOC) in its F/96 mode has the potential to provide highly accurate relative positions for the four quasar components and the lensing galaxy. The images were reduced using the updated geometric corrections appropriate for data taken after 1995 March 19. Table 1 lists the J2000 positions for the four components from a MERLIN map using 1404+286 as a calibrator (Patnaik et al. 1992a). Columns (4)–(7) give the radio offsets measured with respect to component B, and the optical offsets measured from the F480LP image. The F/96 plate scale has been measured with observations of globular clusters to be 0.″01435 ± 0.″0002 pixel^{-1}. For sources with small separations, geomagnetic distortions limit differential astrometry to an accuracy of 0.4 pixels or 0.″0057. Relative positions of the four quasar components measured on the F342W and F480LP images are in close agreement, with a mean difference of Δ(F480LP − F342W) = 0.″004 ± 0.″006. The relative positions between the F480LP image and the MERLIN map are also in excellent agreement, with a mean difference of Δ(F480LP − VLBI) = −0.″004 ± 0.″010. IRAF's *apphot* yields a formal error for the centroid of the lens on the F480LP image of only 0.3 pixels or 0.″0048. If we add this in quadrature to the error caused by geomagnetic distortion, we conclude that the relative position of the lens with respect to the quasar images is accurate to 0.″008. A more conservative error of 0.″010 is given by the rms agreement between relative FOC and MERLIN positions.

3.2. *Photometry*

FOC observations were made through the F342W and F480LP filters. The F342W filter is close to a Johnson *U*; the F480LP filter approximates Johnson *V*, where the upper wavelength of the bandpass is dictated by the falloff in sensitivity of the bialkali photocathode material. Count rates were converted into instrumental magnitudes using the inverse sensitivities 2.92×10^{-18} ergs cm^{-2} Å^{-1} (F342W) and 4.83×10^{-18} ergs cm^{-2} Å^{-1} (F480LP), assuming a spectrum that is flat in F_λ across the bandpass. The F342W images are background-limited, with a sky brightness fainter than 22.9 *U* mag arcsec^{-2}, and the F480LP observations are sky-limited, with a measured sky brightness of 20.7 *V* mag arcsec^{-2}. Instrumental magnitudes are also scaled by a format-dependent correction factor. All photometry was carried out using the IRAF routine *apphot*.

Columns (2)–(3) of Table 2 list the F342W and F480LP

TABLE 1

ASTROMETRY OF THE B1422+231 SYSTEM

	J2000 POSITION		MERLIN[a]		*HST*/FOC[b]	
IMAGE (1)	R.A. (2)	decl. (3)	Δ(R.A.) (4)	Δ(decl.) (5)	Δ(R.A.) (6)	Δ(decl.) (7)
A	$14^h24^m38^s.1219$	+22°56′00.″905	−0.″388	−0.″320	−0.″388	−0.″331
B.....	14 24 38.0938	+22 56 00.585	0	0	0	0
C.....	14 24 38.0696	+22 55 59.837	+0.334	+0.748	+0.337	+0.757
D	14 24 38.1616	+22 55 59.781	−0.937	+0.804	−0.968	+0.789
Lens	14 24 38.1457	+22 55 59.945	...	...	−0.717	+0.640

[a] Radio astrometry based on 5 GHz MERLIN image.
[b] Optical astrometry measured on F480LP image. Differential astrometry with FOC is accurate to 0.″008.

TABLE 2

PHOTOMETRY OF THE B1422+231 SYSTEM

	HST/FOC[b]		Ground-based Imaging			Optical Flux Ratio			Radio[e]
Image[a]	m_{F342W}	m_{F480LP}	V[d]	g[e]	r[e]	m_{F480LP}	V[c]	g[d]	Flux Ratio
(1)	(2)	(3)	(4)	(5)	(6)	(7)	(8)	(9)	(10)
A.....	20.08	17.09	16.71	16.92	16.77	0.79	0.79	0.77	0.98
B.....	19.66	16.84	16.46	16.64	16.45	1.00	1.00	1.00	1.00
C.....	20.34	17.50	17.26	17.44	17.25	0.54	0.48	0.62	0.52
D.....	23.70	20.90	20.42	20.56	20.40	0.024	0.026	0.027	0.020
Lens	23.6	21.6	...	>22.4	21.8	...	...	...	...

[a] D component magnitudes and flux ratio corrected for lens contamination.
[b] Radio flux ratio at 5 GHz from Patnaik et al. 1992b.
[c] Data from Remy et al. 1993.
[d] Data from Yee & Ellingson 1994.
[e] Absolute errors in quasar magnitudes are 0.1 mag due to the FOC spectrophotometric calibration; absolute errors in lens magnitudes are 0.3 mag due to variations in background level. Magnitudes are measured in a 15 pixel (0″.215) radius aperture, adjusted brighter by 0.08 mag (F342W) and 0.06 mag (F480LP) to reflect total magnitudes. Flux ratios are accurate to 2%–3%.

magnitudes for the four quasar components and the lensing galaxy. The quasar images are unresolved. Since the two brightest quasar images are separated by only 36 pixels or 0″.517, the fluxes are integrated out to a radius of 15 pixels or 0″.215. Quasar component fluxes are adjusted brighter by 0.08 mag (F342W) and 0.06 mag (F480LP) to account for the small amount of flux that is missed beyond a radius of 15 pixels (from Table 8 of the FOC Instrument Handbook, Version 6.0, 1995 June). The discovery spectrum of the quasar (Patnaik et al. 1992a) yields a synthetic color of $B - V = 1.50$. This color corresponds to a K5 III spectral type, and the synthetic photometry program FOCSIM gives a color term of $V = m_{F480LP} - 0.16$. Columns (4)–(6) of Table 2 have the published photometry of Remy et al. (1993) and Yee & Ellingson (1994). Columns (7)–(10) list the flux ratios from the three measurements that approximate V passbands (a color term of $V = g - 0.2$ can be assumed), and the original radio flux ratios. The absolute agreement between the three optical observations is good, especially since the absolute FOC calibration is only accurate to about 10%. Although B1422+231 is a compact radio source, there is no evidence for strong optical variations.

Photometry of the lens is more challenging, since it lies close to the glare of quasar light that is 100 times brighter. However, the high resolution of the FOC in its F/96 configuration provides good separation between the lens and all the quasar components. The point spread function (PSF) is determined using component C of the quasar only. Components A and B were not used because the wings of the images merge, and the cores of the images are either nonlinear or saturated. Variations in the PSF across the small F/96 field of view are expected to be negligible, so we can apply the PSF fit to component C across the FOC image. The PSF is fitted out to a radius of 30 pixels or 0″.431. The procedure of PSF fitting and subtraction was characterized by measuring the image core (a radius of 3 pixels or 0″.043), and two regions around the core: an inner annulus extending from 3–9 pixels (0″.043–0″.129), and an outer annulus extending from 9 to 15 pixels (0″.129–0″.215). The lens magnitude is an aperture magnitude integrated out to 30 pixels.

The PSF fit to component C was used to subtract out the core of component D. The residuals were only 1% (F342W) and 6% (F480LP) of the core flux. At large radii, the test could not be performed on component D because of the proximity of the lens. Therefore, we measured the residuals from the fit to component C itself. In the F342W filter, the PSF fitting and subtraction of component C reduced the amount of light in the inner annulus from 30% to 2%–3%, and in the outer annulus from 9% to 1%–2%. In the F480LP filter, the PSF fitting and subtraction reduced the light in the inner annulus from 31% to 1%–2%, and in the outer annulus from 5% to 1%. The PSF model is therefore effective in removing ~94% (F342W) or ~91% (F480LP) of the flux in an unresolved image. Similarly, the lens contributes light to the aperture magnitude for component D. We have measured this contamination, assuming only that the lens light is azimuthally symmetric, with the conclusion that ~16% (F342W) and ~14% (F480LP) of the 15 pixel radius flux is due to the lens. The contamination in the smaller spectroscopic aperture (0″.13 radius) is correspondingly smaller, ~7% (F342W) and ~6% (F480LP). The continuum fluxes for component D in Tables 2 and 3 have been adjusted accordingly.

Systematic errors in the photometry of the lens are dominated by the nearby faint component D. The bright components A, B, and C are far enough away that they contribute an undetectable amount of light at the position of the lens; the relative intensity 0″.5 away from the image core is less than 10^{-4}. The success of the PSF model just described implies that component D can be subtracted with a precision of 5%–10% from under the lens. The lens magnitudes after subtraction of quasar component D are given in Table 2. To convert to the Johnson system, we note that the nominal $U - V$ corresponds to a K0 III spectral type. Synthetic spectra have been used to calculate color terms between the Johnson and FOC filter systems by Paltoglou & Bell (1991). We derive $U - V = m_{F342W} - m_{F480LP} + 0.1 = 2.1$ and $V = 21.4$. At this level sky noise and other systematic errors in the photometry become significant. The errors in the V magnitude and $U - V$ color of the lens are given by the rms variation of the sky background, measured within a 15 pixel radius aperture.

3.3. *Spectroscopy*

The spectrum of image D was approximately corrected for contamination by the lens using the estimates of the previous section and the quasar's color, $U - V = 2.8$, derived from the

TABLE 3

SPECTRAL QUANTITIES OF THE B1422+231 SYSTEM

Image	Radio[a] Flux Ratio	Continuum[b] Flux (ergs s^{-1} cm^{-2} $Å^{-1}$)	Continuum Flux Ratio	Lyα[c] EW (Å)	Lyα Flux (ergs s^{-1} cm^{-2})	Lyα Flux Ratio
A.....	0.98	6.31×10^{-16}	0.78	435 ± 5	$3.11 \pm 0.02 \times 10^{-13}$	0.90
B.....	1.00	8.04×10^{-16}	1.00	377 ± 5	$3.44 \pm 0.03 \times 10^{-13}$	1.00
C.....	0.52	4.01×10^{-16}	0.50	374 ± 7	$1.68 \pm 0.02 \times 10^{-13}$	0.49
D.....	0.020	2.02×10^{-17}	0.025	423 ± 20	$9.18 \pm 0.20 \times 10^{-15}$	0.027

[a] Radio flux ratio at 5 GHz from Patnaik et al. 1992b.
[b] Flux ratio measured from 6110–6350 Å to 1320–1372 Å in the rest frame, although the FOS 0.″26 diameter circular aperture. D/B flux ratio corrected for lens contamination to component D.
[c] Errors in Lyα equivalent widths and fluxes due to continuum placement only.

spectrum of Patnaik et al. (1992a) (extrapolated to both blue and red wavelengths). Given these and the mean flux of image D in the V band, measured by integrating the FOS spectrum, of 2.7×10^{-17} ergs s^{-1} cm^{-2} $Å^{-1}$, the galaxy's flux at the position of image D is estimated to be 1.6×10^{-18} ergs s^{-1} cm^{-2} $Å^{-1}$ at 5400 Å and 1.4×10^{-19} ergs s^{-1} cm^{-2} $Å^{-1}$ at 3500 Å. The galaxy's spectrum was approximated as linear from 3500 Å to ~6800 Å, the long-wavelength cutoff of the FOS spectra, and subtracted from the spectrum of image D.

The mean flux of the FOS spectra of each image was measured in the wavelength range 6110–6350 Å, corresponding to the rest wavelength interval from 1320 to 1372 Å, a region reasonably free of strong emission lines. The fluxes and flux ratios are listed in Table 3. As shown in Figure 2, the spectra are strikingly similar, consistent with the overwhelming evidence in support of a gravitational lens interpretation of this system. The spectra of components A, C, and D were cross-correlated against that of B with the result that the measured shifts between the spectra are all less than 150 km s^{-1}. Data at wavelengths shortward of 5600 Å were excluded from the calculation to avoid the influence of the sharp features of the Lyα forest on the kurtosis of the cross-correlation function. With the FOS, we are able for the first time to cleanly measure spectra of all four components. A detailed analysis of the spectra is deferred to a future paper.

Inspection of the individual spectra showed that the equivalent width of the Lyα + N v emission feature varies from component to component. The equivalent widths and line fluxes of this feature were measured relative to a flat (in F_λ) continuum whose level was set by the mean flux in the wavelength range 5910–5990 Å rest, just shortward of the Si IV λ1400 emission line and the emission feature was integrated over the range 5450–5890 Å. A sample continuum level is show for the spectrum of component D in Figure 2 and the measured equivalent widths and line fluxes are tabulated in Table 3 along with errors arising from the 1 σ error in the continuum placement.

4. DISCUSSION

The equivalent width differences seen in Table 3 could arise from two causes: (1) reaction of the broad emission line region (BLR) to a change in the ionizing continuum or (2) microlensing effects. For the equivalent width differences between images A and B to be explained by the former, the lag between a continuum change and the emission line region's reaction to it must be shorter than the light travel delay between the two images. Since the images of A and B are nearly merging, the delay predicted between the two images is very short at $3.8 \pm 1.0 h_{100}^{-1}$ hr (Hogg & Blandford 1994), probably too small to be reconciled with BLR models. Differential amplification of the continuum source relative to the BLR by microlensing can induce equivalent width variations, although the impact parameter for images A and B is relatively large so the optical depth to microlensing is expected to be small. If microlensing is at work, use of the broadband flux ratios to constrain the macrolens model is compromised; instead, the Lyα flux ratios (Table 3) should be used. Regardless of the explanation, the fact that the emission feature is of different strength in the individual spectra and lies near the center of the V band means that variations in the continuum flux will not result in achromatic photometric variations.

The clear detection of the lens with $V = 21.5 \pm 0.3$ and $U - V = 2.1 \pm 0.6$ is a new constraint on models of the B1422+231 system. Hammer et al. (1995) have published a lens redshift of $z = 0.647$. Since the lens is fainter than component D in the V band, this redshift must be confirmed. Yee & Ellingson (1994) used a color limit of $g - r > 1.4$ to argue that the lens must be an early-type galaxy at $z > 0.35$. They also derived less than 0.75 from a simple point mass deflector model and the requirement that $M/L > 3$. Using the tabulations of galaxy colors as a function of redshift of Fukugita, Shimasaku, & Ichikawa (1995), we find that the lens is too red to be a late-type galaxy at any reasonable redshift. Synthetic spectra yield $U - V < 0.75$ for Sbc galaxies at $z > 0.4$, and $U - V < 1.45$ for Sab galaxies at $z > 0.4$. The best match for ellipticals is a $M_V = -21.5$ galaxy at $z \sim 0.4$, which has a predicted color of $U - V = 1.8$. At the putative redshift of $z = 0.65$, the expected lens would be too faint ($V = 23.8$) and too blue ($U - V = 1.2$).

The FOC images are not deep enough for detailed surface photometry, but simple structural information can be derived. The high resolution allows the lens core to be isolated. The mean surface brightness within a radius of 0.″1 in the F480LP image is 20.3 V mag $arcsec^{-2}$. Correcting for cosmological surface brightness dimming (assuming $z = 0.65$), and adopting a rest frame color of $U - V = 1.5$, the emitted central surface brightness is 16.7 V mag $arcsec^{-2}$, consistent with an elliptical galaxy. The effective radius is $3.1 \pm 0.8 h_{100}^{-1}$ kpc. The raw image was too noisy for isophote fitting, so a 7×7 pixel median filter was applied. Surface photometry of the lens using the VISTA package yielded an ellipse fit at a 9 pixel radius with $1 - b/a = 0.27 \pm 0.13$ at a position angle of $121° \pm 15°$. Note that this is close to the direction of the tangential shear between quasar components A, B, and C. The axis ratio is therefore $a/b = 1.37 \pm 0.14$. The available photometry points to a luminous elliptical at $z \sim 0.4$.

Hogg & Blandford (1994) and Korman, Schneider, & Bartelmann (1994) have published models of the B1422+231 system. The image geometry suggests that the source is close to a cusp singularity, with the three bright images magnified by a combined amplification of ~29, and the faint image D demagnified. Since all observations agree in finding the flux ratio of D to B to be 0.02–0.03, this can be achieved in the models by moving the lens closer to component D, consistent with our new accurate determination of the lens centroid. All optical continuum observations find the ratio of A to B to be 0.77–0.79, leaving the similarity of the A and B fluxes at radio wavelengths unexplained. Korman et al. (1994) produce the image geometry with a highly aspheric deflector. We can rule out the axis ratio predicted by all their models, $1.68 < a/b < 2.86$. The alternative, suggested by Hogg & Blandford (1994), is that shear is contributed by two nearby galaxies, G2 and G3. This requires these two galaxies to be very massive, which can be confirmed by future observations. We conclude by pointing out that simple lens models are still successful under an increasing number of observational constraints. The B1422+231 system remains an excellent cosmological tool.

We thank Tim Pickering for assistance with VISTA, and the referee, Chris Kochanek, for helpful comments. We acknowledge the persistence of Anuradha Koratkar at STScI, and useful conversations with Laird Close, Jens Hjorth, Paul Hewett, Geraint Lewis, and Paul Schechter. C. D. I. and C. B. F. are grateful for the hospitality of the Department of Astronomy, University of Washington, and the Institute of Astronomy, Cambridge University, respectively. This project was supported by STScI grants under the GO Programs 5692 and 5699.

REFERENCES

Fukugita, M., Shimasaku, K., & Ichikawa, T. 1996, ApJ, in press
Hammer, F., Rigaut, F., Angonin-Williams, M.-C., & Vanderriest, C. 1995, A&A, 298, 737
Hogg, D. W., & Blandford, R. D. 1994, MNRAS, 268, 889
Korman, R., Schneider, P., & Bartelmann, M. 1994, A&A, 286, 357
Lawrence, C. R., Neugebauer, G., Weir, N., Matthews, K., & Patnaik, A. R. 1992, MNRAS, 259, 5P
Paltoglou, G. & Bell, R. A. 1991, MNRAS, 253, 449
Patnaik, A. R., Browne, I. W. A., Walsh, D., Chaffee, F. C., & Foltz, C. B. 1992a, MNRAS, 259, 1P
Patnaik, A. R., Browne, I. W. A., Wilkinson, P. A., & Wrobel, J. M. 1992b, MNRAS, 254, 655
Patnaik, A. R., & Porcas, R. W. 1995, in Astrophysical Applications of Gravitational Lensing, ed. C. S. Kochanek & J. N. Hewitt (Dordrecht: Kluwer), 305
Refsdal, S. 1964, MNRAS, 128, 295
Remy, M., Surdej, J., Smette, A., & Claeskens, J.-F. 1993, A&A, 278, L19
Yee, H. K. C., & Ellingson, E. 1994, AJ, 107, 28